



Roles of the Rlim–Rex1 axis during X chromosome inactivation in mice

Feng Wang^{a,1} , Ashmita Chander^{b,1}, Yeonsoo Yoon^c, Janelle M. Welton^b , Mary C. Wallingford^{b,2}, Carmen Espejo-Serrano^d , Francisco Bustos^{d,3} , Greg M. Findlay^d , Jesse Mager^b , and Ingolf Bach^{a,4}

Edited by Jeannie Lee, Massachusetts General Hospital, Boston, MA; received August 1, 2023; accepted November 17, 2023

In female mice, the gene dosage from X chromosomes is adjusted by a process called X chromosome inactivation (XCI) that occurs in two steps. An imprinted form of XCI (iXCI) that silences the paternally inherited X chromosome (Xp) is initiated at the 2- to 4-cell stages. As extraembryonic cells including trophoblasts keep the Xp silenced, epiblast cells that give rise to the embryo proper reactivate the Xp and undergo a random form of XCI (rXCI) around implantation. Both iXCI and rXCI require the lncRNA *Xist*, which is expressed from the X to be inactivated. The X-linked E3 ubiquitin ligase Rlim (Rnf12) in conjunction with its target protein Rex1 (Zfp42), a critical repressor of *Xist*, have emerged as major regulators of iXCI. However, their roles in rXCI remain controversial. Investigating early mouse development, we show that the Rlim–Rex1 axis is active in pre-implantation embryos. Upon implantation Rex1 levels are downregulated independently of Rlim specifically in epiblast cells. These results provide a conceptual framework of how the functional dynamics between Rlim and Rex1 ensures regulation of iXCI but not rXCI in female mice.

X chromosome inactivation | extraembryonic ectoderm | Rlim/Rnf12 | Rex1/Zfp42 | implantation

Eutherian female mammals adjust the gene dosage from X chromosomes between sexes by a process known as X chromosome inactivation (XCI), a paradigm for the study of epigenetic gene silencing. In mice, XCI occurs in two waves. Beginning at the late two-cell/early four-cell stage, imprinted XCI (iXCI) exclusively silences the paternal X (Xp). While extraembryonic cell types including trophoblasts maintain this XCI pattern, cells in the inner cell mass (ICM) specifically reactivate the Xp (XCR) and undergo a random form of XCI (rXCI) around implantation, where each cell inactivates either the maternal X (Xm) or the Xp (1, 2). The long non-coding RNA (lncRNA) *Xist* represents a key regulator of both rXCI and iXCI. *Xist* RNA paints the inactive X from which it is expressed, thereby triggering downstream repressive chromatin modifications including H3K27me3 that lead to X-silencing (3).

In mice, the X-linked *Rlim* (Rnf12) gene encodes a RING finger E3 ligase that is crucial for iXCI (4, 5). Female pre-implantation embryos lacking *Rlim* (KO) display severe inhibition of *Xist* transcription and defective X dosage compensation, and die shortly after implantation due to defective placental trophoblast development (5, 6). Rlim exerts its activity to induce *Xist* by proteasomal targeting of Rex1 (reduced expression gene 1) (7), a gene expressed in undifferentiated embryonic stem cells (8, 9). Rex1 functions as a transcriptional repressor of *Xist* (7), and in female mice, the *Rlim* KO phenotype including iXCI is rescued in *Rlim/Rex1* double KO animals (10), illustrating the critical function of the Rlim–Rex1 axis in controlling iXCI.

During pre-implantation development, Cdx2-induced trophectodermal cells (TEs) form the first epithelium as the outside layer of the embryo (11). At the blastocyst stage, TEs are segregated into mural and polar TE (mTE; pTE) with pTE cells located in close proximity to the ICM. Upon implantation, mTE cells quickly differentiate into trophoblast giant cells (TGCs) that form the parietal yolk sac. In contrast, pTE cells contribute to most placental trophoblast cell types and give rise to the extraembryonic ectoderm (exe) structure that harbors and maintains this progenitor cell type. The pTE progenitor state requires Fgf4 (12–14), which is synthesized by epiblast cells, and its receptor Fgfr2c (15) through mitogen-activated protein kinase (MAPK) signaling via Raf/Mek/Erk (16–18). This pathway activates a transcription factor network that includes Cdx2, Esrrb, Eomes, and Elf5 among others (19–24). Trophoblast development requires X dosage compensation, as deletion of *Xist* in female embryos results in loss of pTEs (25). However, the involved mechanisms leading to this phenotype remain unclear. Moreover, despite major functions in female pre-implantation embryos, the developmental dynamics of Rlim–Rex1 expression and the precise defects caused by axis disturbance are unknown. This issue is

Significance

The ubiquitin ligase Rlim in conjunction with its substrate protein Rex1 are crucial regulators of X chromosome inactivation (XCI), the transcriptional silencing of one X chromosome, required for successful female mouse embryogenesis. However, their contribution toward this process in specific mouse tissues has been controversial. Here, we demonstrate a crucial functional interaction of the Rlim–Rex1 axis during pre-implantation stages for the development of the extraembryonic ectoderm in females. We show further that in contrast to extraembryonic tissues, the functionality of this axis is severed specifically in epiblast cells upon implantation. Thus, a functional Rlim–Rex1 axis is required for X dosage compensation specifically in extraembryonic tissues of female mice.

Author contributions: F.W., J.M., and I.B. designed research; F.W., A.C., Y.Y., J.M.W., M.C.W., C.E.-S., F.B., and J.M. performed research; C.E.-S., F.B., and G.M.F. contributed new reagents/analytic tools; F.W., A.C., J.M., and I.B. analyzed data; and F.W. and I.B. wrote the paper.

The authors declare no competing interest.

This article is a PNAS Direct Submission.

Copyright © 2023 the Author(s). Published by PNAS. This article is distributed under [Creative Commons Attribution-NonCommercial-NoDerivatives License 4.0 \(CC BY-NC-ND\)](https://creativecommons.org/licenses/by-nc-nd/4.0/).

¹F.W. and A.C. contributed equally to this work.

²Present address: Mother Infant Research Institute, Tufts Medical Center, Boston, MA 02111.

³Present address: Department of Pediatrics, Sanford Research, Sioux Falls, SD 57104.

⁴To whom correspondence may be addressed. Email: ingolf.bach@umassmed.edu.

This article contains supporting information online at <https://www.pnas.org/lookup/suppl/doi:10.1073/pnas.2313200120/-DCSupplemental>.

Published December 19, 2023.

particularly important as evidence in mice indicates that *Rlim* is dispensable for rXCI in mice (26), but current models require doses of *Rlim* transcribed from two X chromosomes for activating *Xist* during rXCI (1). Thus, as these ESC-derived models appear incompatible with the in vivo data, the roles of the *Rlim*–*Rex1* axis in epiblast cells remain unclear.

We show that lack of X dosage compensation in female mouse embryos causes cell fate confusion specifically of pTE progenitors, leading to pre-gastrulation lethality. Comparing the dynamic expression of *Rlim* and *Rex1*, we find an inverse correlation of both proteins during pre-implantation development, consistent with crucial functions during iXCI. However, this functional connection is severed upon implantation specifically in the epiblast cell lineage, allowing for *Rlim*-independent rXCI. Our data provide a developmental justification for a strict requirement of X dosage compensation early during mouse embryogenesis and resolve underlying mechanisms of how iXCI but not rXCI is selectively regulated by a dynamic interplay between *Rlim* and *Rex1*.

Results

***Rlim* Activity Is Required Specifically in pTE Precursor Cells in the Exe.** We first examined the precise and sex-specific developmental consequences of disrupting the *Rlim* gene with an emphasis on trophoblast cell types. To efficiently generate embryos lacking *Rlim*, we crossed females carrying a maternal *Sox2*-*Cre*-mediated *Rlim* cKO and a paternal *Rlim* KO allele (*Rlim* flox_m/KO_p; *Sox2*-*Cre*^{+/-}) with males lacking *Rlim* (KO/Y; *SI Appendix, Fig. S1A*). This mating strategy ensures that all offspring lack *Rlim* (6, 26). As our previous studies suggested that lack of *Rlim* has no major effect on pre-implantation development (5), we started out by interrogating female blastocyst outgrowths, comparing them to males that do not undergo XCI and served as controls. Blastocysts were isolated at E3.5 and cultured up to 5 d. The sex was determined via PCR, after image recording. On day 1 of culturing, mTEs stained *Cdx2*⁺ and no obvious differences were observed between female and male embryos (*SI Appendix, Fig. S1B*). At 3 d in culture both male and female embryos had hatched, with similar numbers of

mTE-derived differentiated giant cells, as previously reported (5). Moreover, overall rates of mitosis and cell death at this stage appeared not significantly different between sexes as judged by staining with antibodies against proliferation marker phosphohistone 3 (pH3) (*SI Appendix, Fig. S1B*) or apoptosis marker cleaved Caspase 3 (26). However, *Cdx2* was detectable but with notably decreased signal in female embryos. On day 5, all male outgrowths (n = 14) but none of the females (n = 12) displayed an outgrowth likely consisting of pTE-derived cells (*SI Appendix, Fig. S1 B and C*). These results are consistent with published results (5, 26) and suggest that major developmental effects caused by lack of *Rlim* are in pTE-derived cell types, specifically in females.

To visualize embryonic structures including the epiblast (epi), exe, and ectoplacental cone (epc), we continued our analyses on dissected early post-implantation embryos at developmental stages E5.5 and E6.5. While epiblast tissues, epiblast lumenogenesis, and mTE-derived parietal yolk sac were present both in male and female embryos, presumed pTE-derived trophoblast domains appeared disorganized in 100% of females examined (Fig. 1 *A* and *B*). Using whole-mount in situ hybridization or IF on sections of embryos within decidua failed to detect exe markers including *Wnt7b* (27, 28), *Esrrb* (22, 29), *Eomes* (24), and *Cdx2* (11, 30) (Fig. 1 *C–E*). The lack of these markers that are normally expressed in specific exe subdomains suggests a complete absence of pTE-derived cell types that make up the exe. In contrast, *Oct4*⁺ (31, 32) epiblast tissue was present (Fig. 1*E*), indicating exe-specific defects in *Rlim* null female embryos. These results are fully consistent with data obtained in female embryos with a paternally inherited mutated *Xist* allele (25).

Lack of *Rlim* Causes Cell Fate Confusion of pTE Precursor Cells. Even though the exe structure is entirely absent in *Rlim* KO females, pTE-derived cells appear present albeit at low quantity (Fig. 1*A*). Examining these tissues, we tested expression of *Mash2* (29, 33) a marker for spongiotrophoblast cell types in the epc using whole embryo in situ hybridization. Interestingly, while some female embryos exhibited strong staining comprising the entire trophoblast domain, partial/intermediate or no/weak *Mash2* staining was

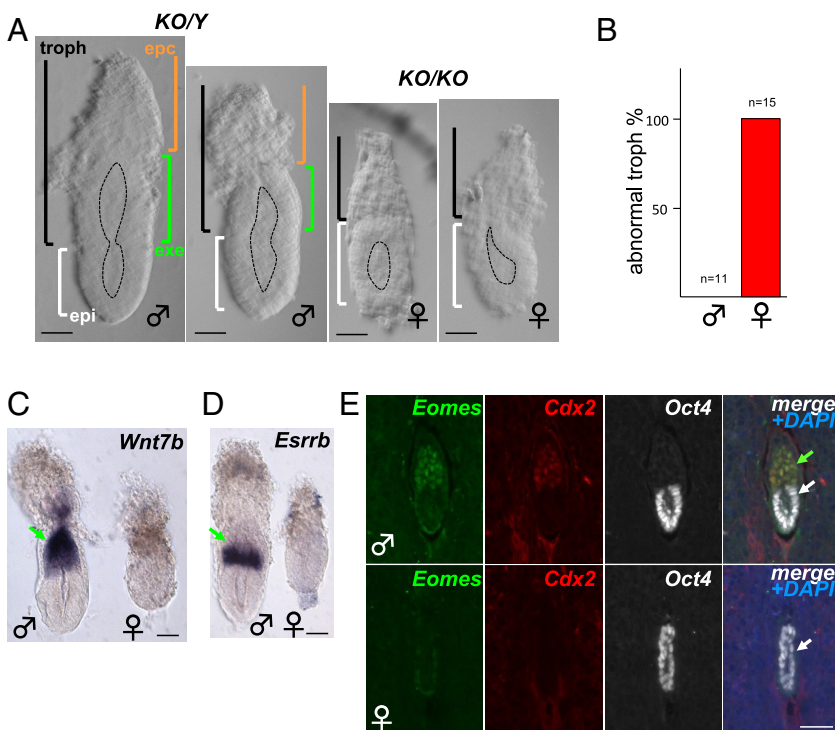


Fig. 1. Absence of the exe structure in female embryos lacking *Rlim*. Male/female littermates within subfigures are shown at the same magnification. Sex was determined after image recording. (A) Representative brightfield images of E5.75 embryos. Approximate embryo and lumen domains are indicated. n > 27 each. epc = ectoplacental cone region (brown); exe = extraembryonic ectoderm region (green); troph = trophoblast-derived (black); epi = epiblast (white). (Scale bars: 60 μ m.) (B) Quantification of phenotypic appearance. (C and D) Whole embryo in situ hybridization. Lack of exe markers *Wnt7b* (C) and *Esrrb* (D) in E5.75 *Rlim* KO females (n > 10, each). (Scale bars: 60 μ m.) (E) IHC of *Rlim* KO embryonic sections at E5.5 within decidua reveals lack of exe markers *Eomes* and *Cdx2*. (Scale bar: 40 μ m.) In (C–E), green and white arrows indicate exe and epiblast regions, respectively.

detected in others (Fig. 2A), and these Mash2 expression patterns appeared in similar frequencies (Fig. 2B). We also noted that many female embryos lacking *Rlim* did not develop a defined epiblast-trophoblast boundary and that Oct4⁺ cells were detectable well into the trophoblast domain (Figs. 1E and 2C). Because Fgf4 expressed by epiblast cells is crucial for the maintenance of pTE progenitor cells (14), we tested Fgf4 expression in female embryos via whole embryo in situ hybridization. Indeed, while the Fgf4 signal in males was more robust, female embryos at E6.5 still expressed Fgf4 mRNA, even though cells in the trophoblast compartment expressing activated phospho-Erk1,2 (p-Erk) were no longer detectable (Fig. 2D and E). Thus, loss of pTE progenitors occurs in the presence of Fgf4, indicating a cell-autonomous requirement of X dosage compensation by this cell type. Combined with published results, these data suggest that lack of Rlim inhibits iXCI (5, 6), leading to pTE progenitor cell fate confusion and premature differentiation into various cell types including the Mash2⁺ spongiotrophoblast lineage.

Inverse Correlation of Rlim and Rex1 Protein Expression in Pre-Implantation Embryos. Next, we investigated the underlying mechanisms for this phenotype and the roles of the Rlim–Rex1 axis by examining the expression profiles of both proteins during pre-implantation development. To obtain high-quality antibodies, we developed a polyclonal Rex1 antibody raised in sheep recognizing aa 1–288 of mouse Rex1 (34). Indeed, when tested on male embryonic stem cell (ESC) models by western blot or by immunostaining, the Rex1 antiserum recognized Rex1 in nuclei of WT ESCs and ESCs lacking *Rlim*, but not ESCs carrying an additional Rex1 deletion (*SI Appendix, Fig. S2 A and B*, respectively). The levels of Rex1 detected in single *Rlim* KO ESCs were increased when compared to WT cells, consistent with Rlim’s E3 ligase activity regulating Rex1 levels (7). These results reveal not only a high specificity of the Rex1 antiserum but also illustrate that the Rlim–Rex1 axis is active in male ESCs.

To illuminate the dynamics of Rlim and Rex1 expression during iXCI in vivo, we performed co-immunostaining on whole embryos, using this Rex1 antibody in conjunction with a previously described

rabbit antibody recognizing the N-terminal portion of Rlim (35), comparing animals lacking *Rlim* (*SI Appendix, Fig. S1A*) with WT controls. We first focused our analyses on whole pre-implantation embryo stages E2.5, E3.5, and E4.5. Because *Rlim* is among X-linked genes that are quickly silenced during the iXCI process, it is mostly expressed from the maternal allele at these stages in both sexes (36), and thus, *Rlim* effects on Rex1 levels in male and female embryos are comparable. As previously reported (5, 26), in WT embryos Rlim is expressed throughout pre-implantation development (Fig. 3). Likewise, Rex1 expression was low but detectable in these embryos at all stages (Fig. 3), with strictly nuclear localization. At E2.5, Rex1 protein was also detected in specific nuclear punctae which, as judged by comparison with DAPI staining, did not correspond to centric heterochromatin domains. Rlim localization in cells was somewhat more diffuse indicating nuclear and some cytoplasmic localization, suggesting shuttling between these compartments (37), co-localizing with Rex1 in the nucleus. Starting at E4.5, general Rlim immunoreactivity specifically in the ICM harboring epiblast cells appeared lower (Fig. 3), when compared to trophoblasts as previously reported (26). Because we detected elevated Rex1 immunoreactivity in embryos lacking *Rlim* throughout pre-implantation development that appeared to peak at E3.5 (Fig. 3), we focused further analyses at this stage. Evaluating a published single embryo RNA-seq dataset (6) revealed similar *Zfp42* (Rex1) mRNA levels in male and female E3.5 embryos with or without Rlim (*SI Appendix, Fig. S3A*). However, quantification of IHC Rex1 signals via ImageJ revealed that low levels of Rex1 protein are Rlim-dependent both in cells of the ICM and trophoblasts irrespective of sex (*SI Appendix, Fig. S3 B and C*). The Rlim–Rex1 protein expression profiles at pre-implantation stages are consistent with a gradual upregulation of Rex1 mRNA from low levels at the 4-cell stage to high levels at blastocyst stages (38) and indicate that the Rlim–Rex1 axis is active throughout pre-implantation development in most/all cells of the embryo.

Rlim-Independent Downregulation of Rex1 Specifically in Epiblast Cells of Implanting Embryos. The role of Rlim in the initiation of *Xist* transcription during rXCI is controversial. Based

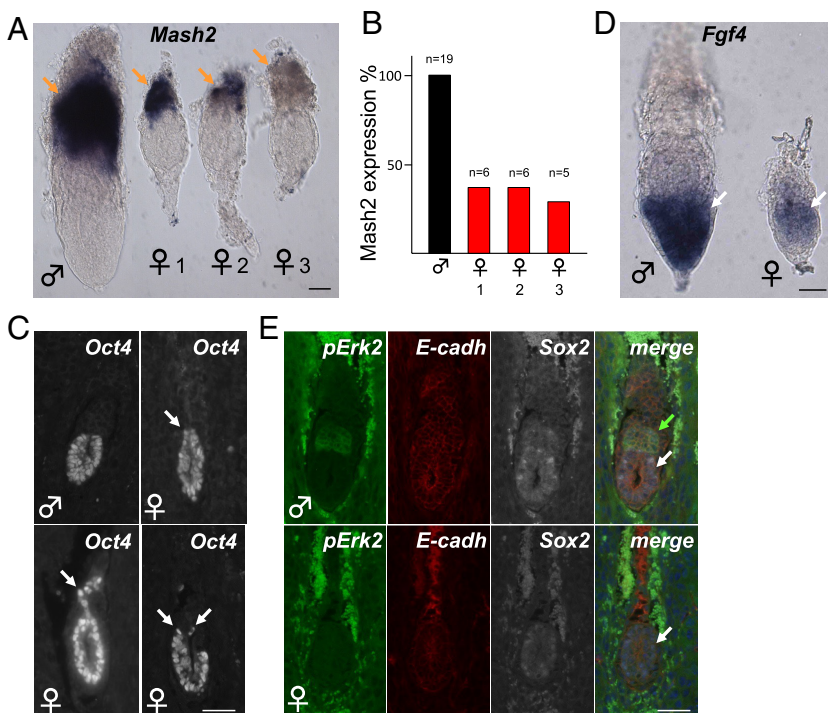


Fig. 2. Lack of iXCI causes pTE cell fate confusion. Representative images of male and female *Rlim* KO littermate embryos at E6.5. Genotyping after image recording. (A) Whole mount in situ hybridization with epc marker Mash2 reveals female embryos with strong (1), intermediate (2), and weak/no staining (3). (Scale bar: 50 μ m.) (B) Summary of (A). (C) Examples of undefined epi/troph border and/or expansion of Oct4⁺ cells into trophoblast domains (arrows, IHC). (Scale bar: 40 μ m.) (D) In situ hybridization of embryos at E6.5 using Fgf4 antisense probe. Note expression of Fgf4 in the epiblast of female *Rlim* KO embryos. (Scale bar: 50 μ m.) (E) Absence of pErk2⁺ cells in *Rlim* KO females (IHC). Same magnification of images within sub-figures. (Scale bar: 40 μ m.) Brown arrows = epc or epc-like; white arrows = epiblast or epiblast-like; green arrow = exe.

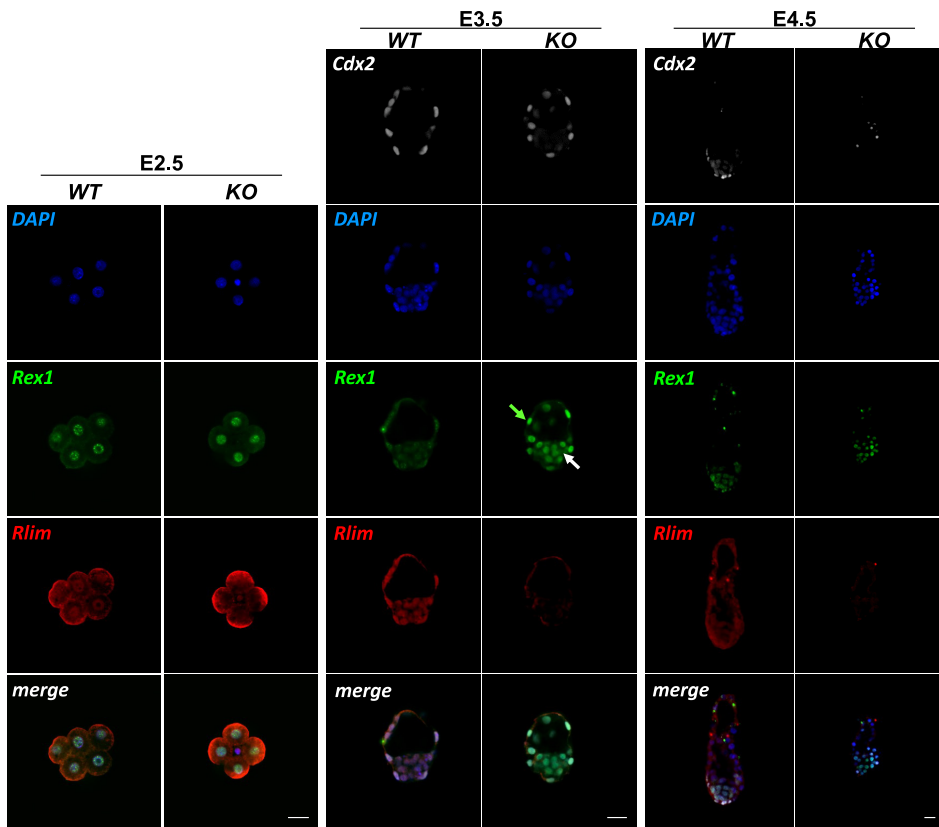


Fig. 3. Increased Rex1 levels in pre-implantation embryos lacking Rlim. WT and *Rlim* KO embryos at stages E2.5, E3.5, and E4.5 were co-stained in parallel using indicated antibodies. Image recordings/processing of KO and control embryos were carried out with the same settings. Rlim = red; Rex1 = green; Cdx2 = white. DAPI = blue. Green and white arrows indicate trophoblast and epiblast regions, respectively. Note elevated Rex1 immunoreactivity in embryos lacking *Rlim* in cells of both regions. (Scale bars: 25 μ m.)

on data from ESCs, the current model of triggering rXCI requires Rlim to be expressed from two alleles (1). However, disputing such a model, results obtained by mouse genetics and tetraploid complementation assays have provided evidence that Rlim is dispensable for rXCI during female mouse embryogenesis (26). To further illuminate roles of the Rlim–Rex1 axis during rXCI in vivo, we investigated the dynamics of Rlim and Rex1 expression in post-implantation embryos with an emphasis on epiblast cells. We first interrogated embryo sections in uteri at E5.0, the time point when rXCI is initiated. Co-staining with antibodies against Rlim and Rex1, we found robust Rlim signals in *Cdx2*⁺ trophoblast tissues, whereas in epiblast cells, signals appeared notably weaker, consistent with published data (Fig. 4A) (26). Importantly and in contrast to pre-implantation stages, Rex1 was very low/nearly absent in WT embryos. In embryos lacking Rlim, Rex1 was robustly expressed in *Cdx2*⁺ extraembryonic tissues, indicating continued roles of Rlim in the turn-over of Rex1, but specifically in *Cdx2*-negative cells, Rex1 levels appeared downregulated. To address the lineage of these cells, we performed co-staining with the epiblast cell marker Oct4. Indeed, our results reveal an Rlim-independent downregulation of Rex1 levels in Oct4⁺ epiblast cells (Fig. 4B), consistent with a functional uncoupling of the Rlim–Rex1 axis specifically in this cell type.

To further investigate the kinetics of this uncoupling process as well as possible influences of sex, we interrogated E5.25 embryos. Again, Rlim immunoreactivity was robust in extraembryonic tissues, with reduced staining in epiblast cells (Fig. 5A and B). Independent of sex, Rex1 was very low/undetectable in WT embryos at this stage both in embryonic and extraembryonic tissues. Importantly, while extraembryonic tissues in the *Rlim* cKO continued to exhibit increased Rex1 levels, Rex1 was very low in Oct4⁺ cells of both male and female embryos (Fig. 5B). Indeed, out of 10 embryos tested, we detected weak Rex1

staining in epiblast cells in only two embryos lacking Rlim at this stage (Fig. 5B). Quantification of Rex1 signals via ImageJ confirmed robust stabilization of Rex1 in Rlim KO trophoblast cells, but levels Oct4⁺ epiblast cells were only slightly above those of WT embryos (compare Fig. 5 and *SI Appendix*, Fig. S4). Examining whole embryos at post-implantation stages E5.5 and E6.5 revealed that low levels of Rex1 continue to be dependent on Rlim in trophoblast but not in epiblast tissues (*SI Appendix*, Fig. S5). Combined, these data are consistent with a rapid differentiation-induced downregulation of Rex1 mRNA (8, 9) and reveal the functional uncoupling of the Rlim–Rex1 axis specifically in epiblast cells, initiated before E5.0 in a sex-independent manner.

Rlim-Independent Downregulation of Rex1 in Epiblast Cells Allows for XCI. Because in female ESCs, high levels of Rex1 inhibit XCI (7), we addressed the question if the Rlim-independent downregulation of Rex1 in epiblast cells would allow for XCI. Thus, we investigated the state of XCI in female embryos lacking *Rlim* by RNA FISH, hybridizing with a probe specifically recognizing the *lncXist* that paints the inactive X chromosome, and by staining sections of embryos in decidua with antibodies against H3K27me3, a downstream marker of *Xist* (3). Because some female *Rlim* KO/KO embryos survive until E7.5 (5), which corresponds to the earliest stage when H3K27me3 foci induced by rXCI are detectable in the epiblast (26), we interrogated the state of XCI in female embryos at this stage. Indeed, all female embryos lacking Rlim ($n = 10$) displayed *Xist* clouds (Fig. 6A and *SI Appendix*, Fig. S6) or H3K27me3 foci in epiblast but not trophoblast tissues (*SI Appendix*, Fig. S7). Combined, these results demonstrate that the Rlim-independent downregulation of Rex1 in epiblast cells allows for the induction of XCI, consistent with findings that *Rlim* is required for iXCI

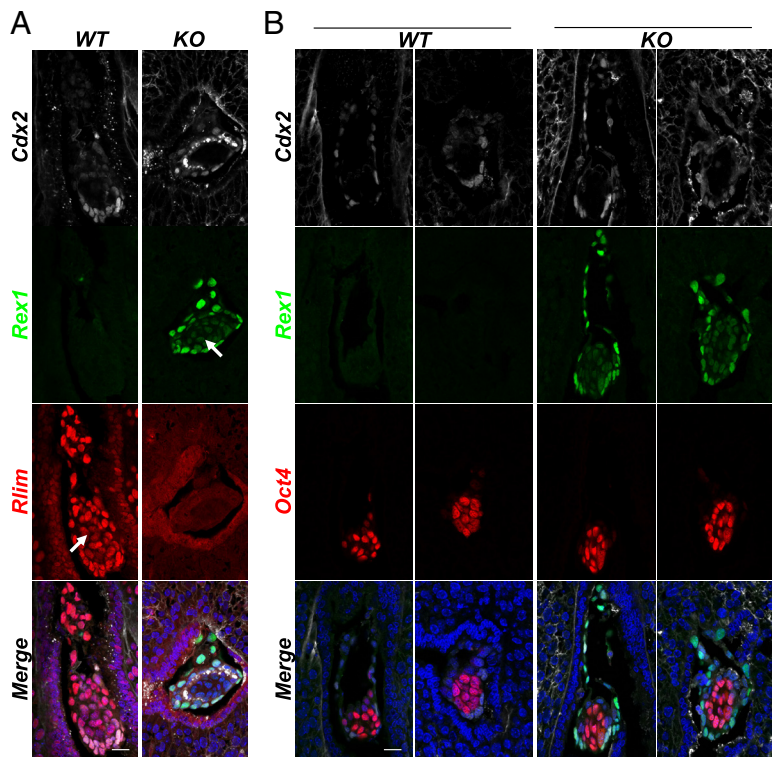


Fig. 4. *Rlim*-independent downregulation of *Rex1* in epiblast cells upon implantation. Sections of WT and *Rlim* KO embryos in uteri at post-implantation stage E5.0 were co-stained in parallel using indicated antibodies. Image recordings/processing of KO and control embryos were carried out using the same settings. (A) Co-staining *Rlim* and *Rex1*. (B) Co-staining *Oct4* and *Rex1*. White arrows indicate epiblast domains. Note decreased *Rex1* immunoreactivity specifically in *Oct4*⁺ epiblast regions in embryos lacking *Rlim*. (Scale bars: 50 μ m.)

but not rXCI (26). These results combined with data showing *Xist* clouds transiently developing during iXCI in female embryos lacking *Rlim* at E2.5 when *Rlim* mRNA and protein levels are low (Fig. 3) (6, 38), provide a conceptual framework of how the *Rlim*–*Rex1* axis regulates iXCI but not rXCI in mice. In this *in vivo* model the activation of *Xist* and XCI is dependent on levels of *Rex1* below specific threshold levels, irrespective of whether *Rlim* is present (Fig. 6B).

Discussion

In female embryos lacking *Rlim*, pre-implantation embryogenesis including the specification and development of initial trophoblast and epiblast tissues appears normal, but a highly penetrant lethal embryonic phenotype precipitates upon implantation (5, 6). While general post-implantation development is severely stalled, the epiblast cell lineage does not appear to display major defects, as female

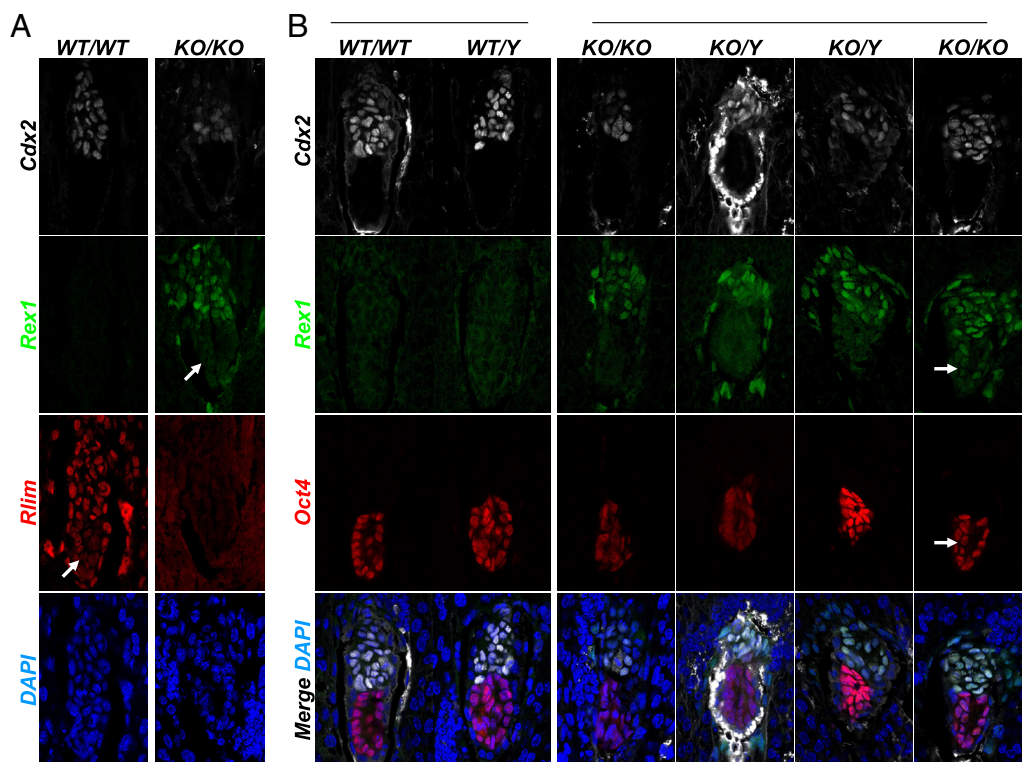


Fig. 5. Low levels of *Rex1* in epiblast cells of embryos lacking *Rlim* by E5.25. Sections of WT and *Rlim* KO embryos in uteri at post-implantation stage E5.25 were co-stained in parallel using indicated antibodies. Image recordings/processing of KO and control embryos were carried out in parallel using the same settings. (A) *Rlim* = red; *Rex1* = green; *Cdx2* = white; DAPI = blue. White arrows indicate epiblast domains. (B) *Oct4* = red; *Rex1* = green; *Cdx2* = white; DAPI = blue. Note low *Rex1* immunoreactivity specifically in epiblast regions in embryos lacking *Rlim*. Arrow points at the epiblast region in an embryo lacking *Rlim* displaying detectable levels of *Rex1* (2 out of 10). (Scale bars: 50 μ m.)

epiblast tissues lacking *Rlim* undergo lumenogenesis (Fig. 1), downregulate *Sox2* expression (Fig. 2), develop *Xist* clouds and H3K27me3 foci (Fig. 6 and *SI Appendix*, Fig. S4), and continue to express *Fgf4* (Fig. 2). Moreover, differentiation of mTE-derived parietal TGCs lacking *Rlim* occurs in a similar fashion to control animals (Fig. 1 and *SI Appendix*, Fig. S1). Thus, the main phenotype in *Rlim* KO female embryos appears mostly restricted to pTE progenitor cells and derived structures. Indeed, pTEs in female embryos lacking X dosage compensation prematurely differentiate without self-maintenance, unable to develop the exo structure. The finding that pTEs cells of some embryos lacking *Rlim* differentiate into *Mash2*⁺ cells but not those in other embryos (Fig. 2) indicates inconsistent differentiation into various cell fates as trophoblast cell lineages other than *Mash2*⁺ spongiotrophoblasts exist that do not express *Mash2*, including the labyrinthine trophoblast lineage (39). The loss of lineage-defining factors including *Cdx2*, *Eomes*, and *Esrrb* (11, 20, 24) in pTEs likely contributes to such cell fate confusion. In this context, considering that reciprocal repression between *Oct4* and *Cdx2* is important for initial trophoblast specification (21), the downregulation of *Cdx2* in female pTEs lacking X dosage compensation (Fig. 3 and *SI Appendix*, Fig. S2) may allow for the reversion of *Oct4* expression in some pTE cells (Fig. 5C). However, even though epiblast cells generally display low migration activity, we cannot exclude that the presence of *Oct4*⁺ cells in trophoblast regions might be caused by migration of cells from epiblast regions. Because the *Rlim*–*Rex1* axis selectively regulates the process of iXCI, the developmental phenotypes observed in females lacking *Rlim* are in strong support of a cell autonomous requirement of X dosage compensation in pTEs. Such a scenario is consistent with the finding that pTEs are also sensitive to *Xist* deletion (25), in contrast to epiblast-derived tissues (40). What makes the pTE progenitor cell lineage particularly vulnerable to X dosage compensation defects? In ESCs, the X dosage influences the pluripotency network via MAPK signaling, and a double dose of X-linked MAPK regulator genes such as *Dusp9* and *Klh113* represses MAPK signaling, thereby activating pluripotency factor expression (41–44). Because MAPK signaling also regulates cell proliferation (14, 45), it is plausible that high levels of X-linked MAPK regulators participate in causing the phenotypes observed in *Rlim* KO pTE progenitors, including inhibition of *Fgf4* signaling, cell proliferation, as well as cell fate confusion (Figs. 1 and 2).

Concerning the functions of the *Rlim*–*Rex1* axis in female pre-implantation embryos, iXCI gradually silences Xp-linked genes until X dosage compensation is reached at late blastocyst stages, including in trophoblast cells (6). The overall pattern of *Rlim* and *Rex1* expression during pre-implantation development in WT controls, combined with elevated *Rex1* levels in *Rlim* KO animals fully support crucial functions of this axis in controlling iXCI, with *Rlim* targeting *Rex1* for proteasomal degradation (7, 10). It is important to point out that *Rex1* protein is low but detectable throughout pre-implantation development in animals WT for *Rlim* (Fig. 3), indicating that much of the process of iXCI occurs in the presence of low levels of *Rex1*. Indeed, signs of *Xist* activation and cloud formation at early stages of mouse pre-implantation development have been reported in females lacking *Rlim* by E2.5 (6), when *Rex1* mRNA levels are low (38). Consistent with this, expression data from animals at E2.5 indicate low levels of *Rex1* protein, with levels only slightly increasing upon deletion of *Rlim* (Fig. 3). In contrast, the requirement for *Rlim* activity to maintain *Rex1* at low levels appears most critical at E3.5, when *Rex1* mRNA expression is high (6, 38). These results are not only fully consistent with whole embryo RNAseq data on *Xist* expression and X-silencing profiles, but also the collapse of *Xist* clouds in female embryos lacking *Rlim* at blastocyst stages (6), indicating that *Rex1* levels in these embryos have reached threshold levels that inhibit *Xist* expression.

With respect to roles of the *Rlim*–*Rex1* axis during rXCI in post-implantation embryos, our results show that the *Rlim*–*Rex1* axis continues to be active in trophoblast tissues. However, in epiblast tissues, this functional interaction is severed by an abrupt *Rlim*-independent downregulation of *Rex1* at the transcriptional level (8, 9), likely initiated at implantation (Fig. 4) and mostly achieved by E5.25, just 6 h after initiation of rXCI (Fig. 5 and *SI Appendix*, Fig. S4). We show further that suppression of *Rex1* levels occurs within a time frame when cells are competent for initiation of *Xist* transcription, allowing rXCI to occur (Fig. 6 and *SI Appendix*, Fig. S7). These results not only provide a molecular explanation of why *Rlim* is not required for rXCI in mice (26), but also a mechanism for the *Rlim*–*Rex1* function specifically in extraembryonic tissues. Combined, these results indicate that activation of *Xist* in female embryos is dependent on doses of *Rex1* below threshold levels during both iXCI and rXCI (Fig. 6C), irrespective of the *Rlim* status.

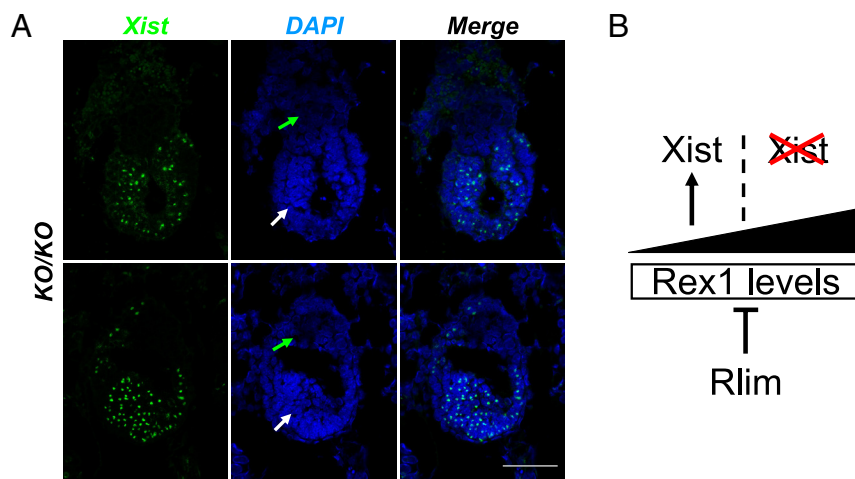


Fig. 6. *Rlim*-independent activation of *Xist* in the embryonic epiblast. (A) RNA FISH on sections of representative *Rlim* KO/KO female embryos in decidua at stages E7.5 using a *Xist* probe. Representative images depicting epiblast and bordering trophoblast embryonic regions. Green and white arrows indicate trophoblast and epiblast regions, respectively. Note the presence of *Xist* paints in epiblast cells but very little trophoblasts. (Scale bars: 20 μ m.) (B) Model of how the *Rlim*–*Rex1* axis regulates iXCI in female mice. *Rlim* activity keeps *Rex1* below threshold levels required for activation of *Xist*. Note that it is the dose of *Rex1* that is critical for activation of *Xist*, whether *Rlim* is present or not.

Regarding rXCI, our results identify important differences between epiblast cells and ESCs with respect to the Rlim–Rex1 axis, as ESCs represent cells at pre-implantation stages when the Rlim–Rex1 axis is active. Thus, varying Rex1 levels in different ESC lines may account for the reported varying degree of Rlim requirement for rXCI in vitro (35, 46). The findings of *Xist* activation in female embryos lacking Rlim appear incompatible with the current ESC-derived model of XCI initiation that requires high Rlim doses expressed from two alleles (1), which needs to be re-evaluated.

In summary, our data show a decisive role of the functional dynamics between Rlim and Rex1 in the control of iXCI but exclude essential functions for rXCI in female mice. Moreover, our results reveal that cell autonomous X dosage compensation via the Rlim–Rex1 axis is required to maintain pTE progenitor cell identity, crucial for successful mouse development.

Materials and Methods

Antibodies. Concerning the generation and characterisation of the REX1 antibody, a sheep anti-mouse REX1 (1-288) antibody was raised by MRC PPU Reagents & Services (MRC PPU R&S code DA136). GST-tagged mouse REX1 (1-288) was used as the immunogen and the serum purified against MBP-tagged REX1 (1-288) to minimise purification of GST antibodies. Antibody specificity was determined by immunofluorescence and immunoblotting. For immunoblotting, *Rlim*^{+/y}, *Rlim*^{-/y} or *Rlim*^{-/-}; *Zfp42*^{-/-} mESCs (47, 48) were cultured on gelatin and lysed in 20 mM tris-HCl (pH 7.4), 150 mM NaCl, 1 mM EDTA, 1% (v/v) NP-40, 0.5% (w/v) sodium deoxycholate, 10 mM β-glycerophosphate, 10 mM sodium pyrophosphate, 1 mM NaF, 2 mM Na₃VO₄, and cOmplete Protease Inhibitor Cocktail Tablets (0.1 U/mL; Roche) and protein extracts resolved by SDS-PAGE prior to transfer. REX1 antibody DA136 (third bleed) was diluted at 1:1,000 and visualized using Donkey anti-Sheep HRP secondary antibody (Thermo Fisher Scientific). Immunoblots were imaged using enhanced chemiluminescence on a BioRad ChemiDoc imager (BioRad). For immunostaining, *Rlim*^{+/y}, *Rlim*^{-/y} or *Rlim*^{-/-}; *Zfp42*^{-/-} mESCs (47, 48) were cultured on gelatin-coated coverslips, fixed with 4% PFA in PBS for 20 min, permeabilized in 0.5% Triton X-100 PBS 5 min and blocked with 1% Fish gelatin PBS 30 min. REX1 antibody DA136 (third bleed) was diluted at 1:1,000 in blocking solution and coverslips were incubated for 2 h. Alexa Fluor 488 Donkey anti-Sheep IgG (Thermo Fisher Scientific) was used as secondary antibody at 1:500 in blocking solution and incubated for 1 h. DNA stain was performed with Hoechst (1:10,000 in PBS) for 5 min. Coverslips were mounted using Fluorsave reagent and imaged using a Zeiss 710 confocal microscope with Zen software (Zeiss). The N-Rlim antibody has previously been described (4, 35). Other commercial primary antibodies were Cdx2 (Biogenex MU392A-UC), pH3 (Millipore NG1740993), Oct4 (Abcam, 200834), E-cadherin (BD biosciences 610181), Eomes (Abcam 23345), H3K27me3 (Millipore Sigma 07-449), pErk1/2 (Cell Signaling #9102), Fgfr2 (Abcam 10648), Casp3 (Cell Signaling #9661), and Sox2 (Abcam 97959). Secondary antibodies were purchased from Thermo Fisher Scientific and include Alexa Fluor® 488 Donkey Anti-Rabbit IgG (A21206), Alexa Fluor® 488 Goat Anti-mouse IgG (A11029), Alexa Fluor® 568 Goat Anti-Rabbit IgG (A-11011), Alexa Fluor® 568 Goat Anti-rat IgG

(A-11077), and Alexa Fluor® 568 Goat Anti-mouse IgG (A-11004), Alexa Fluor® 488 Donkey anti-sheep IgG (A-11015), Alexa Fluor® 546 Donkey anti-Rabbit IgG (A-10040), and Alexa Fluor® 647 Donkey anti-Mouse IgG (A-31571).

Immunostaining of Mouse Embryos. Concerning the determination of embryo stages, noon of the day when mating plugs were observed was considered as embryonic day 0.5 of development (E0.5). Embryo dissections, preparation and culturing of blastocyst outgrowths, and immunostaining of whole mouse embryos, embryonic sections, and blastocyst outgrowths as well as sex determination via PCR was performed as previously described (5, 26). The staining of KO and control embryos were carried out in parallel at each stage, with image recordings and processing performed using the same settings. Statistical analyses were performed using Student's *t* test. The quantification of Rex1 signals on immunostainings was performed using ImageJ, normalized against DAPI on at least two biological replicates.

Whole-Mount In Situ Hybridizations of Mouse Embryos. In situ hybridizations on dissected embryos were performed as previously described (28), including embryo dissections and the preparation and hybridization of probes. Briefly, embryos were dissected at stages E5.5 and E6.5. Noon of the day when mating plugs were observed was considered as embryonic day E0.5. Using forceps, dissections were performed in the dissection medium (DMEM (Gibco) containing 20 mM HEPES, 10% FCS, 100 U/mL penicillin, and 100 µg/mL Streptomycin). Established plasmids have been described for making antisense probes recognizing *Wnt-7b* (28), *Mash2*, *Esrrb*, and *Fgf4* (29).

RNA-FISH. RNA-FISH on sections of mouse embryos within placentae was carried out using a kit (Molecular Instruments) containing an HCR™ Probe (*Xist*, Lot: RTA603), HCR amplifier (B1, Fluorophore Alexa488) and hybridization, wash, and amplification buffers. Sequences for HCR amplifiers B1, B2, B3, B4, and B5 are given in (49). In situ hybridization was performed after sectioning FFPE samples following the Molecular Instruments protocol (<https://www.molecularinstruments.org>).

Data, Materials, and Software Availability. Resources generated in this study are available upon request. All other data are included in the manuscript and/or *SI Appendix*.

ACKNOWLEDGMENTS. We are grateful to K. Tremblay and J. Rossant for sharing plasmids for ISH probes, J. Benanti, T. Fazio, B. Payer, P. Kaufman, and E. Torres for advice and/or discussion. This work was supported by NIH grants R35 GM145263 to I.B. and HD083311 to J.M. and G.M.F. was supported by a Wellcome Trust/Royal Society Sir Henry Dale Fellowship (211209/Z/18/Z) and a Medical Research Council New Investigator Award (MR/N000609/1). I.B. is a member of the University of Massachusetts DERC (DK32520).

Author affiliations: ^aDepartment of Molecular, Cell and Cancer Biology, University of Massachusetts Chan Medical School, Worcester, MA 01605; ^bDepartment of Veterinary and Animal Sciences, University of Massachusetts, Amherst, MA 01003; ^cDivision of Genes and Development, Department of Pediatrics, University of Massachusetts Chan Medical School, Worcester, MA 01605; and ^dMedical Research Council Protein Phosphorylation and Ubiquitylation Unit, School of Life Sciences, University of Dundee, Dundee DD1 5EH, United Kingdom

1. A. Loda, S. Collombet, E. Heard, Gene regulation in time and space during X-chromosome inactivation. *Nat. Rev. Mol. Cell Biol.* **23**, 231–249 (2022).
2. B. Payer, Developmental regulation of X-chromosome inactivation. *Semin Cell Dev. Biol.* **56**, 88–99 (2016).
3. K. Plath *et al.*, Role of histone H3 lysine 27 methylation in X inactivation. *Science* **300**, 131–135 (2003).
4. H. P. Ostendorff *et al.*, Ubiquitination-dependent cofactor exchange on LIM homeodomain transcription factors. *Nature* **416**, 99–103 (2002).
5. J. Shin *et al.*, Maternal Rnf12/Rlim is required for imprinted X-chromosome inactivation in mice. *Nature* **467**, 977–981 (2010).
6. F. Wang *et al.*, Regulation of X-linked gene expression during early mouse development by Rlim. *Elife* **5**, e19127 (2016).
7. C. Gontan *et al.*, RNF12 initiates X-chromosome inactivation by targeting REX1 for degradation. *Nature* **485**, 386–390 (2012).
8. M. B. Rogers, B. A. Hosler, L. J. Gudas, Specific expression of a retinoic acid-regulated, zinc-finger gene, Rex-1, in preimplantation embryos, trophoblast and spermatocytes. *Development* **113**, 815–824 (1991).
9. J. Wang *et al.*, A protein interaction network for pluripotency of embryonic stem cells. *Nature* **444**, 364–368 (2006).
10. C. Gontan *et al.*, REX1 is the critical target of RNF12 in imprinted X chromosome inactivation in mice. *Nat. Commun.* **9**, 4752 (2018).
11. D. Strumpf *et al.*, Cdx2 is required for correct cell fate specification and differentiation of trophoblast in the mouse blastocyst. *Development* **132**, 2093–2102 (2005).
12. B. Feldman, W. Poueymirou, V. E. Papaioannou, T. M. DeChiara, M. Goldfarb, Requirement of FGF-4 for postimplantation mouse development. *Science* **267**, 246–249 (1995).
13. P. A. Latos, M. Hemberger, From the stem of the placental tree: Trophoblast stem cells and their progeny. *Development* **143**, 3650–3660 (2016).
14. S. Tanaka, T. Kunath, A. K. Hadjantonakis, A. Nagy, J. Rossant, Promotion of trophoblast stem cell proliferation by FGF4. *Science* **282**, 2072–2075 (1998).
15. N. Gotoh *et al.*, The docking protein FRS2alpha is an essential component of multiple fibroblast growth factor responses during early mouse development. *Mol. Cell Biol.* **25**, 4105–4116 (2005).
16. E. Arman, R. Haffner-Krausz, Y. Chen, J. K. Heath, P. Lonai, Targeted disruption of fibroblast growth factor (FGF) receptor 2 suggests a role for FGF signaling in pregastrulation mammalian development. *Proc. Natl. Acad. Sci. U.S.A.* **95**, 5082–5087 (1998).
17. V. Bissonauth, S. Roy, M. Gravel, S. Guillemette, J. Charron, Requirement for Map2k1 (Mek1) in extra-embryonic ectoderm during placentogenesis. *Development* **133**, 3429–3440 (2006).

18. M. K. Saba-El-Leil *et al.*, An essential function of the mitogen-activated protein kinase Erk2 in mouse trophoblast development. *EMBO Rep.* **4**, 964–968 (2003).
19. H. J. Auman *et al.*, Transcription factor AP-2gamma is essential in the extra-embryonic lineages for early postimplantation development. *Development* **129**, 2733–2747 (2002).
20. P. A. Latos *et al.*, Fgf and Esrrb integrate epigenetic and transcriptional networks that regulate self-renewal of trophoblast stem cells. *Nat. Commun.* **6**, 7776 (2015).
21. P. A. Latos *et al.*, Elf5-centered transcription factor hub controls trophoblast stem cell self-renewal and differentiation through stoichiometry-sensitive shifts in target gene networks. *Genes Dev.* **29**, 2435–2448 (2015).
22. J. Luo *et al.*, Placental abnormalities in mouse embryos lacking the orphan nuclear receptor ERR-beta. *Nature* **388**, 778–782 (1997).
23. H. Niwa *et al.*, Interaction between Oct3/4 and Cdx2 determines trophoblast differentiation. *Cell* **123**, 917–929 (2005).
24. A. P. Russ *et al.*, Eomesodermin is required for mouse trophoblast development and mesoderm formation. *Nature* **404**, 95–99 (2000).
25. J. W. Mugford, D. Yee, T. Magnuson, Failure of extra-embryonic progenitor maintenance in the absence of dosage compensation. *Development* **139**, 2130–2138 (2012).
26. J. Shin *et al.*, RLIM is dispensable for X-chromosome inactivation in the mouse embryonic epiblast. *Nature* **511**, 86–89 (2014).
27. C. R. Kemp *et al.*, Expression of Frizzled5, Frizzled7, and Frizzled10 during early mouse development and interactions with canonical Wnt signaling. *Dev. Dyn.* **236**, 2011–2019 (2007).
28. Y. Yoon *et al.*, Conditional Aurora A deficiency differentially affects early mouse embryo patterning. *Dev. Biol.* **371**, 77–85 (2012).
29. M. Guzman-Ayala, N. Ben-Haim, S. Beck, D. B. Constam, Nodal protein processing and fibroblast growth factor 4 synergize to maintain a trophoblast stem cell microenvironment. *Proc. Natl. Acad. Sci. U.S.A.* **101**, 15656–15660 (2004).
30. A. Ralston *et al.*, Gata3 regulates trophoblast development downstream of Tead4 and in parallel to Cdx2. *Development* **137**, 395–403 (2010).
31. M. H. Rosner *et al.*, A POU-domain transcription factor in early stem cells and germ cells of the mammalian embryo. *Nature* **345**, 686–692 (1990).
32. H. R. Scholer, S. Ruppert, N. Suzuki, K. Chowdhury, P. Gruss, New type of POU domain in germ line-specific protein Oct-4. *Nature* **344**, 435–439 (1990).
33. F. Guillemot, A. Nagy, A. Auerbach, J. Rossant, A. L. Joyner, Essential role of Mash-2 in extraembryonic development. *Nature* **371**, 333–336 (1994).
34. A. Segarra-Fas *et al.*, An RNF12-USP26 amplification loop drives germ cell specification and is disrupted by disease-associated mutations. *Sci. Signal* **15**, eabm5995 (2022).
35. F. Wang *et al.*, Rlim-dependent and -independent pathways for X chromosome inactivation in female ESCs. *Cell Rep.* **21**, 3691–3699 (2017).
36. M. Borensztein *et al.*, Xist-dependent imprinted X inactivation and the early developmental consequences of its failure. *Nat. Struct. Mol. Biol.* **24**, 226–233 (2017).
37. B. Jiao *et al.*, Functional activity of RLIM/Rnf12 is regulated by phosphorylation-dependent nucleocytoplasmic shuttling. *Mol. Biol. Cell* **24**, 3085–3096 (2013).
38. F. Wang, I. Bach, Rlim/Rnf12, Rex1, and X chromosome inactivation. *Front Cell Dev. Biol.* **7**, 258 (2019).
39. M. Tanaka, M. Gertsenstein, J. Rossant, A. Nagy, Mash2 acts cell autonomously in mouse spongiotrophoblast development. *Dev. Biol.* **190**, 55–65 (1997).
40. L. Yang, J. E. Kirby, H. Sunwoo, J. T. Lee, Female mice lacking Xist RNA show partial dosage compensation and survive to term. *Genes Dev.* **30**, 1747–1760 (2016).
41. J. Choi *et al.*, DUSP9 modulates DNA hypomethylation in female mouse pluripotent stem cells. *Cell Stem Cell* **20**, 706–719.e707 (2017).
42. O. Genolet, A. A. Monaco, I. Dunkel, M. Boettcher, E. G. Schulz, Identification of X-chromosomal genes that drive sex differences in embryonic stem cells through a hierarchical CRISPR screening approach. *Genome Biol.* **22**, 110 (2021).
43. E. G. Schulz *et al.*, The two active X chromosomes in female ESCs block exit from the pluripotent state by modulating the ESC signaling network. *Cell Stem Cell* **14**, 203–216 (2014).
44. J. Song *et al.*, X-chromosome dosage modulates multiple molecular and cellular properties of mouse pluripotent stem cells independently of global DNA methylation levels. *Stem Cell Rep.* **12**, 333–350 (2019).
45. W. Zhang, H. T. Liu, MAPK signal pathways in the regulation of cell proliferation in mammalian cells. *Cell Res.* **12**, 9–18 (2002).
46. T. S. Barakat *et al.*, RNF12 activates Xist and is essential for X chromosome inactivation. *PLoS Genet.* **7**, e1002001 (2011).
47. F. Bustos *et al.*, RNF12 X-linked intellectual disability mutations disrupt E3 ligase activity and neural differentiation. *Cell Rep.* **23**, 1599–1611 (2018).
48. F. Bustos *et al.*, Functional diversification of SRSF protein kinase to control ubiquitin-dependent neurodevelopmental signaling. *Dev. Cell* **55**, 629–647.e627 (2020).
49. H. M. T. Choi, V. A. Beck, N. A. Pierce, Next-generation in situ hybridization chain reaction: higher gain, lower cost, greater durability. *ACS Nano* **8**, 4284–4294. 10.1021/nn405717p.